Nanoscale

Accepted Manuscript

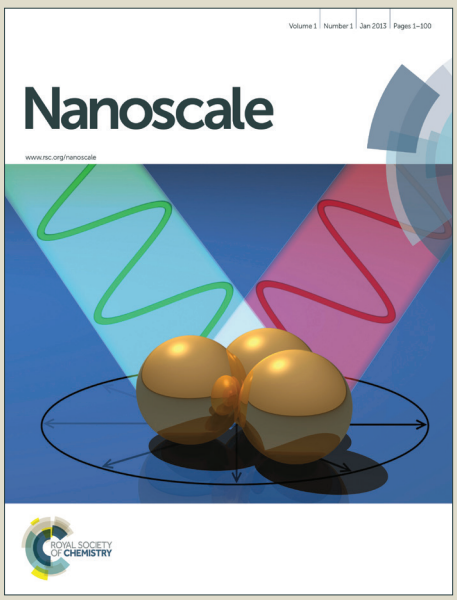

ROYAL SOCIETY OF CHEMISTRY

www.rsc.org/nanoscale

Nanoscale

ARTICLE

Surface engineering on CeO_2 nanorods by chemical redox etching and their enhanced catalytic activity for CO oxidation

Received 00th January 20xx,
Accepted 00th January 20xx

DOI: 10.1039/x0xx00000x

www.rsc.org/

Wei Gao,[a] Zhiyun Zhang,[a] Jing Li,[a] Yuanyuan Ma*[a] and Yongquan Qu*[ab]

Controllable surface properties of nanocerias are desired for various catalysis. It is lack of efficient approaches to adjust the surface properties of ceria to date. Herein, the redox chemical etching method was developed to controllably engineer the surface properties of ceria nanorods. Ascorbic acid and hydrogen peroxide were used to perform the redox chemical etching process, resulting in the rough surface and/or pores on the surface of ceria nanorods. Increasing the etching cycles induced the steady increase of the specific surface areas, oxygen vacancies and surface Ce^{3+} fractions. As a result, the etched nanorods delivered an enhanced catalytic activity for CO oxidation, compared to the non-etched ceria nanorods. Our method provides a novel and facile approach to continuously adjust the surface properties of ceria for the practical applications.

1. Introduction

Nanomaterials are of great interest in various applications, including catalysis, energy conversion and storage, pollutant treatment, drug delivery and sensing.[1-4] The surface properties of materials have significant influences on their performance. Especially for catalysts, the controllable regulation on their surface features is an effective way to enhance their catalytic activity. Surface modifications including the introduction of defects, the formation of composites with metals or metal oxides, the fabrication of porous structures and the exposure of particular crystalline facets *etc.* are broadly employed to improve the catalytic activity of the catalysts.[5-8] For instance, Chen *et al.*[5] reported that the hydrogen treatment on TiO_2 at a high pressure produced the black TiO_2 with a high concentration of the surface oxygen vacancy and a narrow bandgap, which facilitated an enhanced photocatalytic activity for water splitting. Vilé *et al.* has illustrated the relationship between the exposed facets of CeO_2 and their selectivity in the conversion of alkynes to olefins.[6]

Cerium oxide (CeO_2, or ceria), a widely used rare earth oxide, has been extensively explored as the catalytic active species, promoters and supports in areas of catalysis, biomimetics, fuel cells and environmental remediation over the past decades due to the reversible Ce^{3+}/Ce^{4+} redox pair, the rich surface oxygen vacancies and the high oxygen storage capacity.[9-13] Ceria nanocrystals with various morphologies, such as, nanorods,[14] nanooctohedras,[15] nanotubes,[16] nanowires,[17] nanocubes,[18] nanobelts,[19] nanospheres[20] and porous nanostructures[21,22] have been successfully synthesized. In fact, the surface properties of nanocerias, generally dependent on their synthetic methods, are difficult to be adjustable afterwards. Either the chemical doping or the post-treatments including the high temperature annealing have been employed to change the surface properties of nanocerias. However, it is still lack of an efficient method to continuously tune the surface properties of nanocerias.

Herein, we propose a facile wet chemical approach — chemical redox etching method — to realize the controllable surface engineering on the CeO_2 nanorods. Chemical etching is a powerful post-treatment method to change the morphologies of materials while preserve/enhance the properties of the target materials. Through the alternatively treatments on CeO_2 nanorods by L(+)-ascorbic acid (AA)/hydrogen peroxide (H_2O_2) as the reducing agent and oxidant, respectively, the treated CeO_2 nanorods not only delivered a morphology evolution from

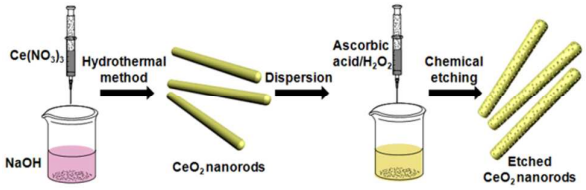

Scheme 1 Synthesis schematic of the CeO_2 nanorods and the chemical reduction/oxidation etching process.

[a] *Center for Applied Chemical Research, Frontier Institute of Science and Technology, and State Key Laboratory for Mechanical Behavior of Materials, Xi'an Jiaotong University, Xi'an, China, 710049. E-mail: yongquan@mail.xjtu.edu.cn; yyma@mail.xjtu.edu.cn. Tel: +86-29-83395357.*
[b] *MOE Key Laboratory for Nonequilibrium Synthesis and Modulation of Condensed Matter, Xi'an Jiaotong University, Xi'an, China 710049.*

† Footnotes relating to the title and/or authors should appear here.
Electronic Supplementary Information (ESI) available: [diameter distributions of as-prepared and etched samples, optical images, specific catalytic data in CO oxidation and comparison of CO oxidation]. See DOI: 10.1039/x0xx00000x

the smooth surfaces into the rough surfaces but also increased the specific surface areas, the concentration of oxygen vacancies and the surface Ce^{3+} fractions. Importantly, the surface properties of the CeO_2 nanorods can be continuously adjustable by increasing the etching cycles. Thus, the present method provides a novel strategy to engineer the surface properties of ceria. It shows the promise to customize the surface properties of ceria for the desired applications.

2. Experimental

All chemicals (AR grade) were used as received, except where otherwise noted. Deionized water used in all experiments was purified with a resistivity of 18.2 MΩ cm.

Synthesis of CeO_2 nanorods. The CeO_2 nanorods were synthesized by a modified hydrothermal method given by Mai *et al*.[14] Briefly, 5 mL of 0.8 M $Ce(NO_3)_3$ solution was added dropwise into 75 mL of 6.4 M NaOH aqueous solution. The mixture was aged at room temperature under continuous stirring for 30 min. Later, the mixture was transferred into a 100 mL Teflon-lined autoclave and kept at 100 ºC for 24 h. After cooling to room temperature, the precipitates were washed by deionized water and ethanol alternatively for three times and dried at 60 ºC overnight.

Chemical redox etching of CeO_2 nanorods. One chemical etching cycle is consist of two steps, namely, the reduction and oxidation of CeO_2 nanorods. To reduce ceria, 500 mg of as-synthesized CeO_2 nanorods were dispersed in 500 mL deionized water by ultrasonic and then 1 mL of 0.5 M ascorbic acid (AA) was added under stirring. After thorough reduction, the reduced nanorods were centrifuged off, washed with deionized water for three times. After re-dispersion of the reduced nanorods in 500 mL of deionized water, 1 mL of 0.5 M H_2O_2 (freshly prepared) was added. After 30-min continuous stirring, the re-oxidized CeO_2 nanorods were centrifuged off and washed by deionized water for three times. Samples with various cycles (namely, 1, 4 and 8 cycles) were obtained by the repeated chemical reduction/oxidation process. All samples were dried at 60 °C overnight.

Characterization. Transmission electron microscopy (TEM) images were obtained from Hitachi HT-7700 with an accelerating voltage of 120 kV. The high-resolution TEM (HRTEM) images were collected on a JEOL-2100F instrument with an accelerating voltage of 200 kV. Powder X-ray diffraction (XRD) patterns were obtained from a Rigaku Powder X-ray diffractometer with the Cu Kα radiation. Specific surface areas were measured on an ASAP 2020 HD 88 (Micromeritics Co.) apparatus by nitrogen physisorption method based on the Brunauer-Emmett-Teller (BET) method. X-ray photoelectron spectra (XPS) were acquired on a Thermo Electron Model K-Alpha with Al Kα as the excitation sources. Ultraviolet-visible (UV-vis) absorption spectra were performed using a PerkinElmer Lambda 35 UV Spectrometer. Raman spectra were recorded by a Renishaw inVia Reflex laser Microprobe Raman spectroscopy using an excitation wavelength of 514 nm.

Catalytic performance in CO oxidation. The activities of samples were performed on a home-made fixed-bed quartz reactor connected to a flow apparatus equipped with mass flow controllers. A mixture gas of 1% CO, 1% O_2 and 98 % Ar was delivered at a flow rate of 25 sccm into the quartz reactor filled with 125 mg catalysts (60-100 mesh). The temperature ramping rate was controlled at 5 ºC/min. An online gas chromatograph equipped with a flame ionization detector (FID) was used to detect the effluent CO and CO_2. The time internal between two temperature points was 30 min to reach steady activity.

The CO conversion was calculated in the following formula:

$$\text{CO conversion} = ([CO]_{in}\text{-}[CO]_{out}) / [CO]_{in} \times 100\%.$$

3. Results and discussion

Synthesis of the CeO_2 nanorods and the chemical redox etching process are schematized in Scheme 1. The CeO_2 nanorods were synthesized *via* a hydrothermal method.[14] The chemical redox etching was performed on the CeO_2 nanorods treated by AA for the reduction reaction and H_2O_2 for the oxidation reaction as a sequence. The etched CeO_2 nanorods were obtained after the multi-cycle treatments, which were denoted as CeO_2-NR-*x* and *x* represented the cycles of the reduction/oxidation process. Details of experiments are given in the experimental section.

TEM and HRTEM images presented the morphology of as-synthesized CeO_2 nanorods and the etched CeO_2 nanorods with various cycles of the chemical reduction/oxidation. As showed in Fig. 1a, as-synthesized CeO_2 nanorods exhibited a smooth surface with a length of ~100 nm and a width of ~ 8.5 ±1.0 nm. (Detailed size distributions are given in Fig. S1, Electronic Supplementary Information, ESI) HRTEM image (inset, Fig. 1a) also demonstrated the high quality of CeO_2 nanorods and their

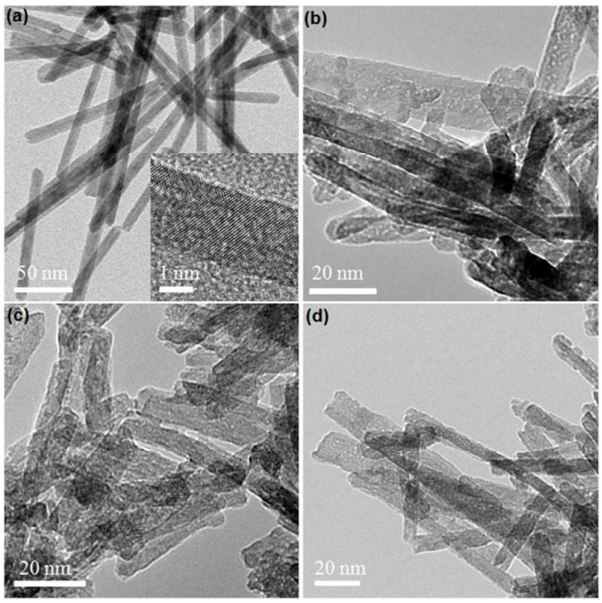

Fig.1 TEM images of CeO_2 nanorods. (a) As-synthesized CeO_2 nanorods (insert: HRTEM of the CeO_2 nanorods). (b) CeO_2 nanorods after (b) one cycle, (c) four-cycle, and (d) eight-cycle oxidation/reduction treatment.

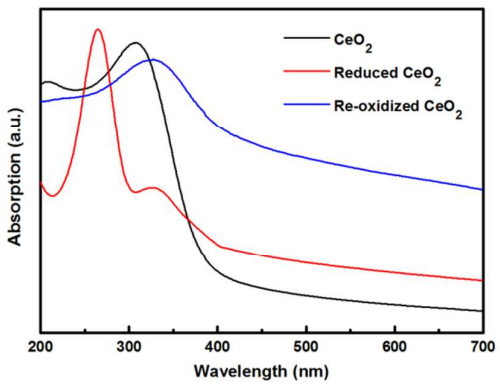

Fig. 2 UV-vis absorption spectra of original CeO_2 nanorods, reduced CeO_2 by ascorbic acid and re-oxidized CeO_2 by hydrogen peroxide.

structural features. After chemical redox etching treatment, the rough surface of the treated CeO_2 nanorods associated with micropores were observed (Fig. 1b-1d), indicating the occurrence of the chemical etching during the post-treatments.

As reported by the previous studies,[23-27] AA can reduce the surface Ce^{4+} into Ce^{3+} and H_2O_2 can re-oxidize Ce^{3+} to Ce^{4+} (Equation 1 and 2), accompanied with the significant changes in color (Fig. S2, ESI).

$$2Ce^{3+} + H_2O_2 \rightarrow 2Ce^{4+} + 2OH^- \quad (1)$$

$$2Ce^{4+} + C_6H_8O_6 \rightarrow 2Ce^{3+} + C_6H_6O_6 + 2H^+ \quad (2)$$

The ultraviolet-visible (UV-vis) absorption spectra in Fig. 2 further confirmed the surface chemical reduction/oxidation reactions. The chemical reduction induced by AA led to the apparent blue-shift in UV-vis absorption profile due to the decrease of Ce^{4+}. While, the oxidization of the reduced CeO_2 nanorods by H_2O_2 resulted in the red-shift in UV-vis absorption

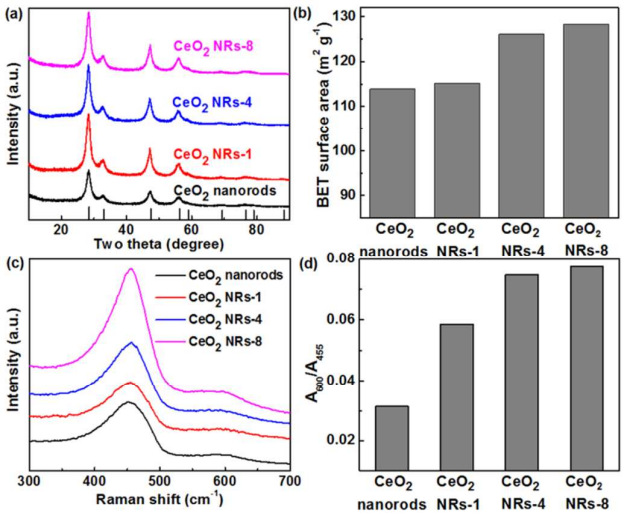

Fig. 3 (a) XRD patterns, (b) specific surface areas and (c) Raman spectra of as-synthesized CeO_2 nanorods and the treated CeO_2 nanorods with various cycles (1, 4 and 8) of the chemical reduction/oxidation. (d) The area ratios of Raman peaks at 455 cm^{-1} and 600 cm^{-1} for all CeO_2 nanorods derived from their Raman spectroscopic profiles shown in c.

Table 1 Structural information of as-synthesized ceria nanorods and etched ceria nanorods

	Diameter (nm)	Specific surface area/m^2 g^{-1}	A_{600}/A_{455} in Raman spectra[a]	Surface Ce^{3+} fraction/%
CeO_2 nanorods	8.5 ± 1.0	113.9	0.0314	17.8
CeO_2 NRs-1	7.4 ± 1.1	115.1	0.0586	19.9
CeO_2 NRs-4	6.5 ± 1.0	126.4	0.0747	23.7
CeO_2 NRs-8	5.8 ± 1.1	128.3	0.0775	27.1

[a] Calculated from the Raman spectra, the integrated peak areas were centred at ~ 455 cm^{-1} and 600 cm^{-1} separately.

curve because of the increase of Ce^{4+}, which came from the oxidation of Ce^{3+}.[23] The formation of the rough surface and micropores can be explained by the dissolution of cerium ions during the reduction/oxidation reactions. Of note, the average values of the diameter of the treated nanorods were 7.4 ± 1.1, 6.5 ± 1.0 and 5.8 ± 1.1 nm (Fig. S1, ESI) for the nanorods after 1, 4 and 8 cycles of the reduction/oxidation treatments, respectively, indicating the phenomenon of the chemical redox etching.

XRD patterns in Fig. 3a illustrated the preservation of the cubic fluorite structure (PDF #34-0394) for the etched ceria nanorods, similar to that of as-synthesized CeO_2 nanorods. Significantly, the surface properties of the etched nanorods can be continuously adjusted by the number of the etching cycles. As summarized in Fig. 3b and Table 1, the specific surface areas of the etched nanorods were 115.1, 126.4 and 128.3 m^2 g^{-1} for CeO_2-NR-1, CeO_2-NR-4 and CeO_2-NR-8, respectively. Compared to that (113.9 m^2 g^{-1}) of the as-synthesized CeO_2 nanorods, the increased surface areas can be attributed to the apparent surface roughness and micropores of the etched nanorods with the increase of etching cycles. Raman spectra in Fig. 3c exhibited that as-synthesized and the etched CeO_2 nanorods had a strong band at ~ 455 cm^{-1} and a weak band at ~ 600 cm^{-1}. The band at ~ 455 cm^{-1} is ascribed to the Raman-active vibrational mode (F_{2g}) of the fluorite-type structure, while the band at ~ 600 cm^{-1} demonstrated the intrinsic oxygen vacancies due to the existence of Ce^{3+} in CeO_2.[28] To study the change in oxygen vacancies, the ratios of the integral areas of the two peaks (namely the ratio of A_{600} and A_{455}, A_{600}/A_{455}) were calculated. As showed in Fig. 3d and Table 1, the ratios of two peaks increased with the increase of the etching cycles, illustrating that more cycles of the chemical reduction/oxidation led to the higher concentration of oxygen vacancies.

To further study the tunability in the surface properties of the treated nanorods by the chemical redox etching, the surface states of the nanorods were further analyzed by the XPS technique. The Ce *3d* spectra and corresponded peak fitting results are given in Fig. 4a. Eight peaks associated with 3d electron of Ce are corresponding to four pairs of spin-orbit doublets.[29-32] The XPS fitting process of Ce *3d* core level was achieved through the method given by previous reports.[29, 30] Peaks marked as u/v, u''/v'' and u'''/v''' are assigned to Ce^{4+} species while peaks denoted as u'/v' are attributed to Ce^{3+} species.[29-32] Calculated from the integrated areas of the respective peaks, the fractions of the surface Ce^{3+} of the treated CeO_2 nanorods steadily mounted-up with the increase of

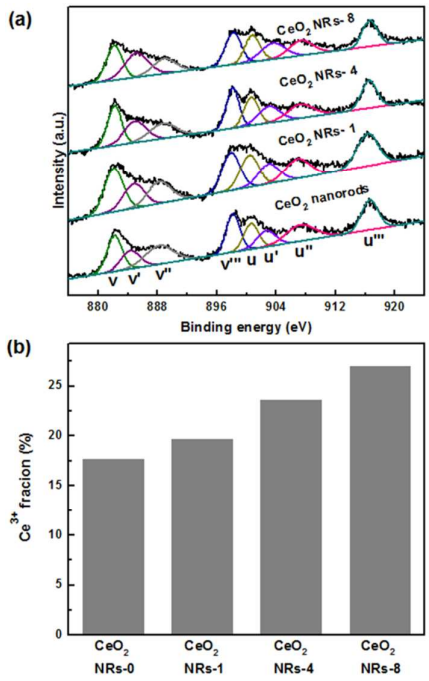

Fig. 4 (a) XPS spectra of the Ce *3d* core level regions, and (b) surface Ce^{3+} fractions of the as-synthesized CeO_2 nanorods and the etched CeO_2 nanorods with 1, 4 and 8 reduction/oxidation cycles, respectively.

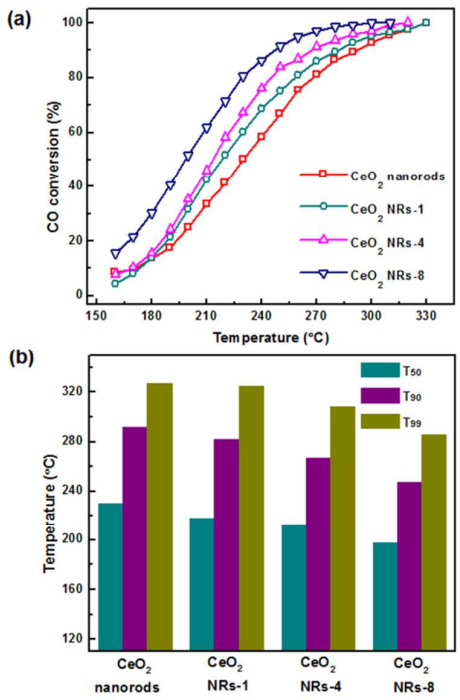

Fig. 5 (a) CO oxidation reaction activity of all catalysts, and (b) critical temperatures (T_{50}, T_{90} and T_{99}) of CO conversion of the original CeO_2 nanorods and the etched CeO_2 nanorods with 1, 4 and 8 redox cycles, respectively.

chemical redox cycles, which was consistent with the changes of the concentration of oxygen vacancies (Fig. 3c and 3d). Therefore, it can be deemed that the chemical reduction/ oxidation etching process not only changes the morphology of nanorods into ones with the rougher surfaces and/or micropores, but also increases the surface Ce^{3+} fractions associated with the increased concentration of oxygen vacancies. Hence, the chemical redox etching provides a direct and facile approach to realize the continuously adjustable surface properties of ceria.

Working as the catalyst, CeO_2 holds the promise as the catalytic converters for exhaust gases and diesel soot and as the highly conductive solid electrolyte for high temperature fuel cells due to its high oxygen mobility and diffusivity in ceria and the reversible electrochemical process.[9,18,33,34] Herein, CO oxidation reaction is chosen as a model reaction to assess the influence of the surface properties of the etched CeO_2 nanorods on their catalytic activity. The CO oxidation reaction on metal oxides are commonly explained by the two-step Mars-van Krevelen mechanism.[22,35] The surface Ce^{3+} sites play a crucial role in the absorption of CO molecules. Then CO is activated by the lattice oxygen to form the intermediate COO*, which is transferred into CO_2 later. The oxygen vacancies are generated accompanied by the release of CO_2, and then reacted with gas-phase oxygen to re-produce surface oxygen atoms.[22,35,36] Obviously, the surface Ce^{3+} fraction and the concentration of oxygen vacancies can significantly affect their catalytic activity, thus CO oxidation is a suitable model reaction to assess the changes of surface properties induced by redox chemical etching process on their catalytic activity.

Fig. 5a shows the light-off curves for CO oxidation over the CeO_2 nanorods, CeO_2-NR-1, CeO_2-NR-4 and CeO_2-NR-8. The reactions for all catalysts were performed under identical conditions. The CeO_2-NR-8 catalysts exhibited the best catalytic activity for CO oxidation, followed by the CeO_2-NR-4, CeO_2-NR-1 and CeO_2 nanorods. The trend of catalytic activity in CO oxidation was consistent with those of the specific surface areas, Ce^{3+} fractions as well as the concentration of oxygen vacancy. The temperatures of 50% CO conversion (T_{50}), 90% CO conversion (T_{90}) and 99% CO conversion (T_{99}) for all samples given in Fig. 5b and Table S1(ESI) further confirmed the catalytic activity of the four catalysts. For example, T_{99} of the CeO_2-NR-8 was 286 °C, which was 41, 39 and 22 °C lower than those of the CeO_2 nanorods, CeO_2-NR-1 and CeO_2-NR-4, respectively. The above catalytic results suggested that more amount of the active sites of the etched nanorods were provided and exposed to the environment for CO oxidation. The highest catalytic activity of the CeO_2-NR-8 ambiguously attributed to its largest surface area of 128.3 m^2 g^{-1} and the highest surface Ce^{3+} fraction of 27.1%.

In order to study the size effect on the catalytic activity of ceria, small ceria nanoparticles (about 5-6 nm, Figure S3a, ESI) synthesized by high temperature calcination on cerium nitrate [22] were used as the catalysts for CO oxidation at the same conditions. The size of ceria nanoparticles is similar to the diameter of CeO_2-NR-8. As given in Fig. S3b, ceria nanoparticles delivered much lower catalytic activity, in which the CO conversion catalyzed by ceria nanoparticles was

significant lower than that by CeO_2-NR-8. The T_{50}, T_{90} and T_{99} for ceria nanoparticle catalysts were 273 ºC, 316 ºC and 341 ºC, respectively, which were 75 ºC, 73 ºC and 55 ºC higher than those of CeO_2-NR-8. The different catalytic activity can be attributed to the different ratios of Ce^{3+}/Ce^{4+}, which are 17.2% and 27.1% for CeO_2 nanoparticles (Fig. S4, ESI) and CeO_2-NR-8, respectively. The results indicate that the ratio of Ce^{3+}/Ce^{4+} plays an important role in catalytic oxidation of CO, consistent with a recent report.[37] Therefore, the activity of the catalysts has a strong correlation to their surface properties, which the large surface area and the high surface Ce^{3+} fraction associated with the high concentration of oxygen vacancies significantly improve their catalytic performance for CO oxidation. In this way, the continuous adjustment in surface properties of CeO_2 nanorods enhanced the catalytic activity gradually.

4. Conclusions

In summary, we present a direct and facile approach to continuously adjust the surface properties of ceria through a chemical redox etching method with ascorbic acid and hydrogen peroxide. With the increased cycles of the reduction/oxidation treatment, the surface properties of the specific surface areas, oxygen vacancies and surface Ce^{3+} fractions of the CeO_2 nanorods are steadily increased. Herein, it provides a novel strategy to realize the controllable surface properties for the desired applications.

Acknowledgements

The authors acknowledge support from the National Nature Science Foundation (21201138, 21401148). This work was also partially funded by the Ministry of Science and Technology of China through a 973-program under Grant 2012CB619401 and by the Fundamental Research Funds for the Central Universities under Grant xjj2013102 and xjj2013043. We gratefully acknowledged the support of Raman spectra from the Center of Nanomaterials for Renewable Energy, School of Electrical Engineering, Xi'an Jiaotong University.

Notes and references

‡ Footnotes relating to the main text should appear here. These might include comments relevant to but not central to the matter under discussion, limited experimental and spectral data, and crystallographic data.

1 V. Valtchev and L. Tosheva, *Chem. Rev.,* 2013, **113**, 6734-6760.
2 Y. Qu and X. F. Duan, *Chem. Soc. Rev.,* 2013, **42**, 2568-2580.
3 R. G. Chaudhuri and S. Paria, *Chem. Rev.,* 2012, **112**, 2373-2433.
4 J. T. Zhang and C. M. Li, *Chem. Soc. Rev.,* 2012, **41**, 7016-7031.
5 X. B. Chen, L. Liu, P. Y. Yu and S. S. Mao, *Science,* 2011, **331**, 746-750.
6 G. Vilé, B. Bridier, J. Wichert and J. Pérez-Ramírez, *Angew. Chem. Int. Ed.,* 2012, **51**, 8620-8623.
7 H. P. Zhou, H. S. Wu, J. Shen, A. X. Yin, L. D. Sun and C. H. Yan, *J. Am. Chem. Soc*., 2010, **132**, 4998-4999.
8 T. Yu, J. Zeng, B. Lim and Y. Xia, *Adv. Mater.,* 2010, **22**, 5188-5192.
9 D. S. Zhang, X. J . Du, L. Y. Shi and R. H. Gao, *Dalton Trans.,* 2012, **41**, 14455-14475.
10 C. W. Sun, H. Li and L. Q. Chen, *Energy Environ. Sci.,* 2012, **5**, 8475-8505.
11 L. Vivier and D. Duprez, *ChemSusChem,* 2010, **3**, 654-678.
12 Q. Yuan, Q. Liu, W. G. Song, W. Feng, W. L. Pu, L. D. Sun, Y. W. Zhang and C. H. Yan, *J. Am. Chem. Soc*., 2007, **129**, 6698-6699.
13 C. T. Campbell and C. H. F. Peden, *Science,* 2005, **309**, 713-714.
14 H. X. Mai, L. D. Sun, Y. W. Zhang, R. Si, W. Feng, H. P. Zhang, H. C. Liu and C. H. Yan, *J. Phys. Chem. B*, 2005, **109**, 24380-24385.
15 I. Florea, C. Feral-Martin, J. Majimel, D. Ihiawakrim, C. Hirlimann and O. Ersen, *Cryst. Growth Des.,* 2013, **13**, 1110-1121.
16 W. Q. Han, L. J. Wu and Y. M. Zhu, *J. Am. Chem. Soc.,* 2005, **127**, 12814-12815.
17 X. H. Lu, D. Z. Zheng, J. Y. Gan, Z. Q. Liu, C. L. Liang, P. Liu and Y. X. Tong, *J. Mater. Chem.,* 2010, **20**, 7118-7122.
18 J. M. Zhen, X. Wang, D. P. Liu, S. Y. Song, Z. Wang, Y. H. Wang, J. Q. Li, F. Wang and H. J. Zhang, *Chem. Eur. J.,* 2014, **20**, 4469-4473.
19 Z. L. Wang, G. R. Li, Y. N. Ou, Z. P. Feng, D. L. Qu and Y. X. Tong, *J. Phys. Chem. C*, 2011, **115**, 351–356.
20 X. Liang, J. J. Xiao, B. H. Chen and Y. D. Li, *Inorg. Chem.,* 2010, **49**, 8188-8190.
21 C. W. Sun, J. Sun, G. L. Xiao, H. R. Zhang, X. P. Qiu, H. Li and L. Q. Chen, *J. Phys. Chem. B,* 2006, **110**, 13445-13452.
22 J. Li, Z. Y. Zhang, Z. M. Tian, X. M. Zhou, Z. P. Zheng, Y. Ma and Y. Qu, *J. Mater. Chem. A,* 2014, **2**, 16459-16466.
23 J. M. Perez, A. Asati, S. Nath and C. Kaittanis, *Small,* 2008, **4**, 552-556.
24 M. Kitsuda and S. Fujihara, *J. Phys. Chem. C,* 2011, **115**, 8808-8815.
25 G. Z. Chen, H. G. Zhao, F. Rosei and D. L. Ma, *J. Phys. Chem. C,* 2013, **117**, 10031-11038.
26 C. J. Lv, W. H. Di, Z. H. Liu, K. Z. Zheng and W. P. Qin, *Analysts,* 2014, **139**, 4547-4555.
27 W. Gao, J. Li, X. M. Zhou, Z. Y. Zhang, Y. Ma and Y. Qu, *J. Mater. Chem. C,* 2014, **2**, 8729-8735.
28 M. Guo, J. Q. Lu, Y. N. Wu, Y. J. Wang and M. F. Luo, *Langmuir,* 2011, **27**, 3872-3877.
29 E. Paparazzo, *Mater. Res. Bull.*, 2011, **46**, 323-326.
30 E. Paparazzo, *Appl. Catal. B: Environ.*, 2011, **105**, 248-251.
31 Z. X. Li, L. L. Li, Q. Yuan, W. Feng, J. Xu, L. D. Sun, W. G. Song and C. H. Yan, *J. Phys. Chem. C,* 2008, **112**, 18405-18411.
32 H. F. Li, G. Z. Lu, D. S. Qiao, Y. Q. Wang, Y. Guo and Y. L. Guo, *Catal. Lett.,* 2011, **141**, 452-458.
33 A. Bueno-López, *Appl. Catal. B-Environ.,* 2014, **146**, 1-11.
34 R. O. Fuentes and R. T. Baker, *Int. J. Hydrogen Energy,* 2008, **33**, 3480-3484.
35 Y. Liu, C. Wen, Y. Guo, G. Z. Lu and Y. Q. Wang, *J. Phys. Chem. C,* 2010, **114**, 9889-9897.
36 R. C. Rao, Q. Y. Zhang, H. D. Liu, M. Yang, Q. Ling and A. M. Zhang, *CrystEngComm*, 2012, **14**, 5929-5936.
37 K. An, S. Alayoglu, N. Musselwhite, S. Plamthottam, G. Melaet, A. E. Lindeman and G. A. Somorjai, *J. Am. Chem. Soc.*, 2013, **135**, 16689-16696.